Journal of
Materials Chemistry B

PAPER

View Article Online
View Journal | View Issue

Cite this: J. Mater. Chem. B, 2016, 4, 7620

Micelle-forming HPMA copolymer conjugates of ritonavir bound *via* a pH-sensitive spacer with improved cellular uptake designed for enhanced tumor accumulation

E. Koziolová, D. Machová, R. Pola, O. Janoušková, P. Chytil, R. Laga, S. K. Filippov, V. Šubr, T. Etrych* and M. Pechar

Received 30th August 2016,
Accepted 3rd November 2016

DOI: 10.1039/c6tb02225a

www.rsc.org/MaterialsB

We describe design, synthesis, physico-chemical characterization and preliminary biological evaluation of micelle-forming polymer drug conjugates with controlled drug release intended for tumor treatment. The structure of the conjugates was designed to enable tumor tissue- and cell-specific drug release and micelle disassembly to avoid side effects accompanying classic chemotherapy and guarantee safe elimination of the drug-free carrier from the organisms. The amphiphilic polymer conjugates consisted of a hydrophobic hexaleucine block and a hydrophilic block based on the *N*-(2-hydroxypropyl)methacrylamide (HPMA) copolymer with an antiviral and cytostatic drug, ritonavir, bound through a pH-sensitive spacer. Diblock copolymers with low dispersity ($Đ \sim 1.1$) were prepared *via* reversible addition-fragmentation chain transfer (RAFT) copolymerization using a hexaleucine derivative as a chain transfer agent. The associative properties of the copolymers depend on the hydrophilic polymer block length and the hydrophobic ritonavir content. The micelles dissociated under mild acidic conditions mimicking the environment inside tumor tissue/cells, because of the decrease in polymer hydrophobicity after the rapid release of the hydrophobic drug from the polymer carrier. Unexpectedly, the polymer–ritonavir conjugates internalized into HeLa cells significantly more than the polymers without ritonavir. The enhanced cell penetration and pH-triggered micelle disassembly predetermine the polymer–ritonavir conjugates to become promising tumor-targeted drug carriers.

1 Introduction

The current neoplastic therapy usually includes the application of low-molecular-weight chemotherapeutics that cause significant toxicity not only to the target cancer cells and tumors but also to healthy cells, tissues and organs. Moreover, these compounds are quickly excreted from the organism, and consequently, only a small part of the applied dose can reach the target tumor cells.

It has been repeatedly reported[1] that the covalent attachment of anti-tumor drugs to a hydrophilic polymer carrier can substantially improve the pharmacokinetics of the drug. This attachment prolongs its circulation in the blood, slows down the excretion and, probably most importantly, increases the concentration of the drug in the tumor due to the enhanced permeation and retention (EPR) of macromolecules in vascularized tumors.[2–4]

Among others, polymer conjugates of various drugs that are usually based on *N*-(2-hydroxypropyl)methacrylamide (HPMA) copolymers have been investigated.[5] The excellent antitumor activity of the polymer–drug conjugates containing the cytostatics doxorubicin, pirarubicin, paclitaxel or docetaxel bound *via* a pH-sensitive spacer that is stable during circulation in blood (pH 7.4) but rapidly hydrolyzes in tumors after a pH decrease to 6 in the tumor microenvironment or to 5–5.5 in endosomes/lysosomes of tumor cells has been shown repeatedly. An efficient uptake of the conjugates by cancer cells and the intratumoral or intracellular release of the free drug are prerequisites for the conjugate activity.[6–8]

Ritonavir, a clinically approved HIV protease inhibitor, also exhibits substantial cytostatic activity against various cancer cells and it has been proved to overcome multidrug resistance in cancer cells.[9–11] Unfortunately, the clinical application of ritonavir in cancer treatment is limited due its poor solubility and non-specific toxicity in healthy cells. Such disadvantages can be overcome by transporting in its inactive polymer carrier-bound form in blood and its subsequent delivery and controlled release in tumor cells.

Institute of Macromolecular Chemistry, Czech Academy of Sciences, Heyrovsky Sq. 2, Prague 6, 162 06, Czech Republic. E-mail: etrych@imc.cas.cz; Fax: +420-296 809 410; Tel: +420-296 809 231

We have recently reported that a ritonavir derivative, ritonavir 5-methyl-4-oxohexanoate (Rit), has a similar biological activity to the parent drug.[12] In this work, we have bound Rit to HPMA copolymers *via* a pH-sensitive hydrazone bond that is relatively stable at neutral pH (in the blood) and hydrolyzed in a slightly acidic environment, such as that of the tumor tissue or inside tumor cells, thus enabling the release of free, active Rit from the carrier.

It was shown that the level of passive accumulation of the conjugates in solid tumors due to the EPR effect depends on the size or the molecular weight of the polymer carrier to a large extent.[13] Due to the larger hydrodynamic radii, the micelle-forming polymer conjugates accumulate in tumor tissue to a significantly higher extent than hydrophilic polymers.[14] In contrast, the larger-sized macromolecular carriers persist in the body for a longer time after delivering the drug because they cannot be easily eliminated through renal filtration. Therefore, it is highly desirable to work with such polymer conjugates that exist as supramolecular objects in blood circulation but disassemble into smaller, easily excretable fragments after the drug is released inside the target cells or tissue. Among the micellar drug delivery systems, stimuli-responsive micelles represent the most advanced and sophisticated technology.[15,16] There are numerous examples of micelles sensitive to changes in temperature,[17,18] pH,[19] light intensity[20] or reducing agents.[21]

We hypothesized that both the structure of the polymer carrier and the presence or absence of the hydrophobic drug (Rit) might influence the association behavior of the copolymers in aqueous medium and their interactions with living cells. For these reasons two types of HPMA-based copolymers (pHPMA), *i.e.* hydrophilic pHPMA and an amphiphilic diblock copolymer consisting of a hydrophilic pHPMA block and a hydrophobic peptide block based on hexaleucine, were conjugated with Rit and compared. They differed in the pHPMA length and the content of the drug. The most representative conjugates were labeled with the fluorescent dye Cyanine5.5 for evaluating the *in vitro* cell internalization. In addition, the corresponding control copolymers of both types without ritonavir were synthesized and characterized.

The major goal of this work was the synthesis, determination of the physico-chemical properties and preliminary biological evaluation of a novel micellar system based on amphiphilic diblock copolymers consisting of a hydrophobic hexaleucine-containing block and a hydrophilic block formed by the HPMA copolymer with Rit attached *via* a pH-sensitive spacer. We expected that the conjugates of the diblock copolymers with Rit were sensitive to the pH changes of aqueous solutions and that the micelles formed by the self-assembly of the copolymers were stable at physiological pH (7.4) and disintegrated relatively quickly upon a drop in pH in a mildly acidic region (pH 5–6) corresponding to the pH of the intracellular environment. After the release of the highly hydrophobic Rit from the polymer carrier, which is a prerequisite for its biological activity,[12] the polymer chains will become less hydrophobic, resulting in the disruption of the supramolecular organization and the formation of the soluble and excretable polymer fragments. The verification of this hypothesis is given in this work. In addition, the results of the study of the cellular uptake of these micelle-forming Rit conjugates *in vitro* are also included.

2 Materials and methods

2.1 Chemicals

1-Aminopropan-2-ol, methacryloyl chloride, 2,2′-azobis(isobutyronitrile) (AIBN), 2-cyanopropan-2-yl dithioate, 4-cyano-4-(thiobenzoylthio)pentanoic acid, dimethyl sulfoxide (DMSO), 1,1,1,3,3,3-hexafluoro-2-propanol (HFIP), 1-hydroxybenzotriazole (HOBt), *tert*-butyl alcohol (*t*-BuOH), and 2,4,6-trinitrobenzene-1-sulfonic acid (TNBSA) were purchased from Sigma-Aldrich. *N*-Ethyldiisopropylamine (DIPEA), *N*,*N*-dimethylformamide (DMF), 9-fluorenylmethoxycarbonyl-amino acids (Fmoc-aa), 2-chlorotrityl chloride resin and (benzotriazol-1-yloxy)trispyrrolidinophosphonium hexafluorophosphate (PyBOP) were purchased from Iris Biotech, GmbH, Germany. Ritonavir was purchased from ChemPacific Corp. Cyanine5.5 *N*-hydroxysuccinimide (NHS) ester was purchased from Lumiprobe. All other chemicals and solvents were of analytical grade. The solvents were dried and purified by conventional procedures.

2.1.1 Synthesis of the monomers. *N*-(2-Hydroxypropyl)-methacrylamide (HPMA) and 1-(*tert*-butoxycarbonyl)-2-(6-methacrylamidohexanoyl)hydrazine (MA-Acap-NHNH-Boc) were prepared as described in ref. 22 and 23, respectively.

2.1.2 Synthesis of the functionalized chain transfer agent. The linear octapeptide 4-cyano-4-(thiobenzoylthio) pentanoyl Val-Ser($\psi^{Me,Me}$pro)–Leu_6 (CTA) was assembled by automatic solid phase peptide synthesis using a Liberty Blue microwave peptide synthesizer (CEM, Matthews, NC, USA), starting from the C-terminus using standard Fmoc procedures with the consecutive addition of the *N*-Fmoc-protected amino acid derivative (2.5 equiv.), PyBOP (2.5 equiv.), HOBt (2.5 equiv.), and DIPEA (5.0 equiv.) in DMF. Amino acid derivatives were coupled in the following order: Fmoc-Leu-OH, Fmoc-Leu-OH, Fmoc-Leu-OH, Fmoc-Leu-OH, Fmoc-Leu-OH, Fmoc-Leu-OH, Fmoc-Val-Ser($\psi^{Me,Me}$pro)-OH and 4-cyano-4-(thiobenzoylthio) pentanoic acid. The Fmoc groups were removed using piperidine–DMF (1 : 4). The loading of the 2-chlorotrityl chloride resin with Fmoc-Leu-OH was determined by spectrophotometric measurements of the Fmoc group (1.5 mmol g^{-1}) released by 25% piperidine in DMF. The cleavage of the protected peptide derivative CTA (Scheme 1) from the resin was performed with 30% solution of HFIP in dichloromethane (15 mL g^{-1} of resin), for 1 h. The resin was filtered off and rinsed with dichloromethane. The filtrate was concentrated under vacuum and precipitated with diethyl ether. The precipitate was isolated by filtration and dried in a vacuum, yielding 0.151 g (64%) of the peptide derivative. The product was characterized by Matrix-assisted laser desorption/ionization time-of-flight mass spectrometry (MALDI-TOF MS) (1184.7, M + H) performed on a Bruker BIFLEX III (Bruker Daltonics, Billerica, MA, USA). Reverse-phase high-performance liquid chromatography (HPLC) showed a single peak (Chromolith Performance RP-18e column,

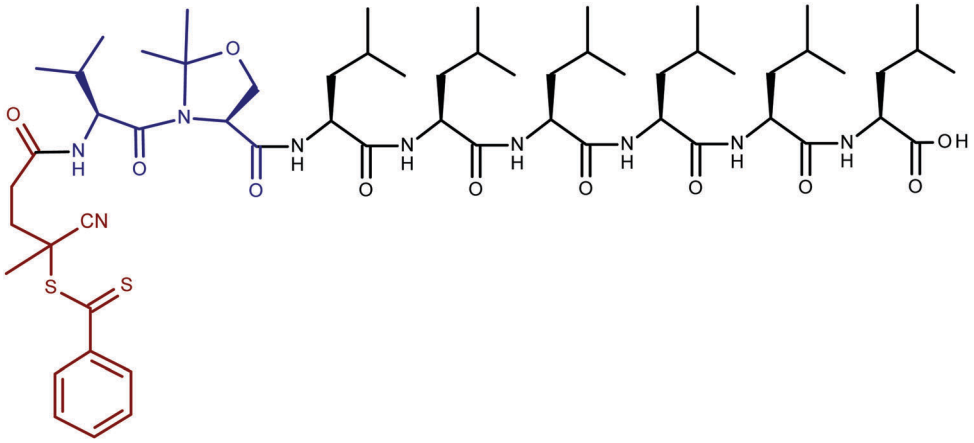

Scheme 1 The structure of octapeptide 4-cyano-4-(thiobenzoylthio) pentanoyl Val-Ser($\psi^{Me,Me}$pro)–Leu_6 (CTA).

100 × 4.6 mm (Merck, Germany), and UV detection at 305 nm was performed using a SPD-M20A photodiode array detector (Shimadzu, Japan)).

2.1.3 Synthesis of the copolymers. The characteristics of the polymer precursors and conjugates are listed in Table 1. The polymer precursors P1 and P2 based on HPMA were synthesized by controlled radical Reversible Addition-Fragmentation chain Transfer (RAFT) polymerization using CTA as a chain transfer agent and AIBN as an initiator. The polymerization was carried out in *t*-BuOH with 20% of DMSO at 70 °C for 16 h. The ratio of monomer : CTA was 70 : 1 or 105 : 1, and the ratio of CTA : AIBN was 2 : 1.

An example of the synthesis of polymer precursor P1 (the molar ratio of monomer : CTA : AIBN = 140 : 2 : 1): HPMA (0.5 g, 3.5 mmol) and MA-Acap-NH-NH-Boc (0.12 g, 0.4 mmol) were dissolved in *t*-BuOH (3.45 mL), and CTA (66 mg, 5.54×10^{-2} mmol) and AIBN (4.6 mg, 2.77×10^{-2} mmol) were dissolved in DMSO (1.72 mL). The solution of CTA and AIBN was added to the monomer solution. The polymerization mixture was added to an ampule, bubbled with argon for 10 min and sealed. The polymerization was carried out at 70 °C for 16 h. The polymer was isolated by precipitation with a mixture of acetone : diethyl ether (3 : 1), filtered off and dried in a vacuum. The yield was 0.26 g (84%). The ω-end dithiobenzoate group (DTB) was removed by a method described by Perrier using AIBN.[24] The hydrazide groups were deprotected according to the literature[22] using trifluoroacetic acid. The pseudoproline protecting group from the peptide was removed in the same step. The content of the hydrazide groups of the polymer precursors was determined by a modified TNBSA assay.[25]

The polymer carrier P3 without Val-Ser–Leu_6 at the polymer chain end was prepared analogically to P1 using 2-cyanopropan-2-yl dithibenzoate as the chain transfer agent.

2.1.4 Synthesis of the polymer conjugates. Ritonavir 5-methyl-4-oxohexanoate (Rit) and all the polymer–Rit conjugates prepared by conjugation of the copolymer precursor with Rit, forming the pH-sensitive hydrazone bond, were prepared according to the literature.[12] The polymer conjugates were isolated by gel filtration on a Sephadex LH-20 column in methanol, followed by precipitation with ethyl acetate. The content of Rit in the polymer conjugates was determined using HPLC after acid hydrolysis as previously described.[12]

The conjugates with the fluorescent dye Cyanine5.5 were synthesized by the reaction of Cyanine5.5 NHS ester with the hydrazide groups on the polymer backbone in methanol overnight. An example of the synthesis of the polymer–dye conjugate FP1 is as follows: P1 (150 mg) was dissolved in dry methanol (1.5 mL), and Cyanine5.5-NHS ester (3 mg) was added to the solution. The reaction mixture was stirred for 16 h at room temperature. The progress of the reaction was monitored by HPLC. The reaction mixture was then diluted with dry methanol (3 mL), and the conjugate FP1 was purified by column chromatography on a Sephadex LH-20 column in methanol using UV/Vis detection at 678 nm. The compound was precipitated with ethyl acetate, isolated by filtration, and dried under vacuum. The content of Cyanine5.5 was determined spectrophotometrically

Table 1 The molecular characteristics of the polymer precursors and conjugates

Sample name	Prepared from	M_w[b] (g mol^{-1})	$Đ$[b]	R_h[c] (nm)	Rit content[d] (wt%)	Dye content[e] (wt%)
P1	—	8900	1.10	2.4	—	—
P1-RitA	P1	11 950	1.10	11.5	4.9	—
P1-RitB	P1	12 800	1.11	9.6	11.0	—
FP1	P1	ND[f]	ND	ND	—	1.5
FP1-Rit	FP1	ND[f]	ND	ND	11.5	1.5
P2	—	25 000	1.10	4.4		
P2-RitA	P2	26 200	1.10	5.3	2.5	—
P2-RitB	P2	27 400	1.10	9.8	9.7	—
P3[a]	—	7530	1.06	2.5	—	—
FP3[a]	P3	ND[f]	ND	ND	—	1.8
FP3-Rit[a]	FP3	ND[f]	ND	ND	11.2	1.8

[a] Copolymers without the Val-Ser–Leu_6 block. [b] Molar weights and dispersity were determined by SEC using multiangle light scattering and refractive index detectors. [c] Hydrodynamic radius was determined by dynamic light scattering. [d] Drug content was determined by HPLC after acid hydrolysis. [e] Dye content was determined spectrophotometrically. [f] GPC profiles of the fluorescently labeled polymers were similar to those of the corresponding polymer precursors; however, the precise calculation of M_w cannot be executed due to the interaction of the LS detector laser with the fluorescent dye.

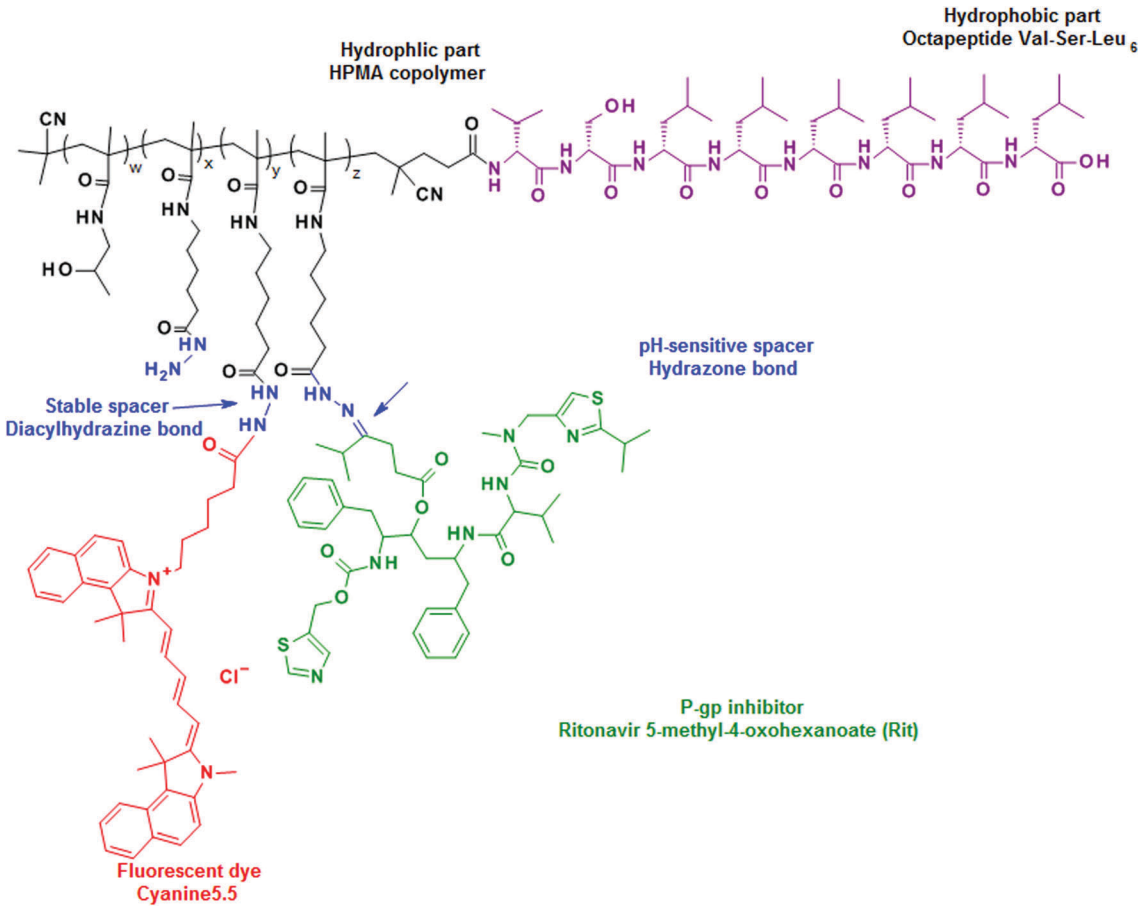

Scheme 2 The structure of the Rit conjugate with Cyanine5.5 containing six leucines (FP1-Rit or FP2-Rit).

(ε_{678} = 250 000 L mol^{-1} cm^{-1} in methanol). The structure of the Rit conjugate with Cyanine5.5 containing six leucines (FP1-Rit or FP2-Rit) is given in Scheme 2.

2.1.5 Characterization of the polymer carriers and the conjugates. The number-average molecular weights (M_n), weight-average molecular weights (M_w), and dispersities ($Đ$) of the polymer precursor and conjugates before Cyanine5.5 attachment were measured using size-exclusion chromatography (SEC) on a HPLC Shimadzu system equipped with a SPD-M20A photodiode array detector (Shimadzu, Japan), an Optilab®rEX differential refractometer and a multi-angle light scattering DAWN® HELEOS II (Wyatt Technology, USA) detector using 0.3 M sodium acetate buffer at pH 6.5 (20%) – methanol (80%, v/v) as the mobile phase and a TSKgel G3000SW column. The ASTRA VI software and the refractive index increment dn/dc = 0.167 mL g^{-1} were used for the calculation.

The hydrodynamic radii (R_h) of the conjugates in a phosphate buffer (5 mg mL^{-1}; pH 7.4, 0.1 M with 0.05 M NaCl) were measured using a Nano-ZS instrument (ZEN3600, Malvern). The intensity of the scattered light was detected at an angle θ = 173° using a laser with a wavelength of 632.8 nm. The DTS (Nano) program was used for the dynamic light scattering data evaluation. The values are equivalent to the mean of at least six independent measurements. The values were not extrapolated to the zero concentration.

The accurate determination of the micellar M_w of non-labeled conjugates was carried out by the static light scattering measurements in the angular range of 30–150° using an ALV goniometer equipped with a 30 mW He–Ne laser (vertically polarized light at λ = 632.8 nm). The Zimm plot procedure was used for the M_w evaluation.

The critical micellar concentration (CMC) values were determined by isothermal titration calorimetry (ITC) using an isothermal titration microcalorimeter MicroCal iTC200. The ITC experiments were performed using 20 injections of the polymer solution in a phosphate buffer at pH 7.4 into the buffer (the titration volume varied during the experiment from 0.5, 1 and 2 μL; 120 s intervals). The thermograms were recorded and analyzed using the Origin 7 software.

Synchrotron SAXS experiments were performed at the B21 beam line (Diamond Light Source, Didcot, UK) using a pixel detector (2M PILATUS). The X-ray scattering images were recorded for a sample-detector distance of 3.1 m using a monochromatic incident X-ray beam (λ = 0.125 nm) covering a range of momentum transfer of 0.05 nm^{-1} < q < 4.5 nm^{-1} ($q = 4\pi \sin\theta/\lambda$, where 2$\theta$ is the scattering angle). Most of the samples had no measurable radiation damage detected by the comparison of twenty successive time frames with 50 ms exposures. In all the cases reported in this work, the two-dimensional scattering patterns were isotropic.

They were azimuthally averaged to yield the dependence of the scattered intensity $I_s(q)$ on the momentum transfer q. Prior to fitting analysis, the solvent scattering was subtracted.

All data manipulations were performed using the PRIMUS software. The forward scattering $I_s(q = 0)$ and the radius of gyration R_g were evaluated using the Guinier approximation. For further modeling, the data were brought to an absolute scale by subtracting an empty cell measurement from a pure water measurement and scaling by the ratio of the theoretical forward scattering of water and the experimental forward scattering intensity of water.

2.1.6 Cell culture. The HeLa cell line was cultivated in Dulbecco's modified Eagle medium (DMEM) supplemented with heat inactivated 10% fetal bovine serum (FCS), 100 U mL^{-1} of penicillin and 100 μg mL^{-1} of streptomycin (Thermo Scientific, Czech Republic). For laser scanning confocal microscopy, the cells (2×10^5 cells) were seeded in 1 mL of media on a 35 mm glass bottom dish with four chambers, a 20 mm microwell, and a #1 cover glass (0.13–0.16 mm) (Bio-Port Europe, Czech Republic) one day before incubation with the polymer conjugates. For flow cytometry, the cells (5×10^4 cells) were seeded in 1 mL of media into 24-well flat-bottom plates (TPP, Czech Republic) one day before incubation with the polymer conjugates.

2.1.7 Internalization of fluorescently labeled polymer conjugates. For the evaluation of the *in vitro* cell internalization of the polymer conjugates, laser scanning confocal microscopy (LCSM) was used. The polymer conjugates were incubated with the cells for 2 h in a 5% CO_2 atmosphere at 37 °C. The amount of fluorescently labeled polymer conjugates added to the cell suspensions was normalized to the Cyanine5.5 content (1 μg mL^{-1}), corresponding to a final conjugate concentration of 111 μg mL^{-1} of FP3 and FP3-Rit, and 83 μg mL^{-1} of FP1 and FP1-Rit.

Prior to the end of the incubation time (10 min), CellMask Green (1000 diluted, Life Technology, Czech Republic) was added to label the cell membrane, and Hoechst 33342 (5 μg mL^{-1}, Thermo Scientific, Czech Republic) was added to label the nucleus. After 2 h, the native cells were washed three times with phosphate buffer saline (PBS). All experiments were carried out in duplicate in four independent experiments.

The polymer-bound Cyanine5.5 dye was excited at 647 nm, and the emitted light was detected through a 650–750 nm filter. For the detection of the CellMask Green-labeled cell membranes, an excitation wavelength of 488 nm and the detection of the emitted light through a 500–600 nm filter were used. To probe for the Hoechst 33342 dye-labeled nuclei, the sample was excited at 405 nm, and emitted light was detected through a 425–500 nm filter. A laser scanning confocal microscope, Olympus IX83, with the FV10-ASW software (Olympus, Czech Republic) was used to observe the fluorescence and transmitted light. The samples were scanned using a 60× oil immersion objective Plan ApoN (1.42 numerical aperture).

2.1.8 Quantification of internalized fluorescently labeled polymer conjugates by flow cytometry. Polymer conjugates were incubated with cells for 2 h in a 5% CO_2 atmosphere at 37 °C. The amount of fluorescently labeled polymer conjugates FP1-RiT and FP3-RiT added to the cell suspensions was normalized to the Rit content (12.8 μg Rit per mL), which corresponded to a final conjugate concentration of 112 μg mL^{-1} of FP1-Rit and 111 μg mL^{-1} of FP3-Rit. The concentrations of the controlled conjugates FP1 and FP3 added to the cells were similar to those of FP1-RiT and FP3-RiT (112 μg mL^{-1} and 111 μg mL^{-1}, respectively). Normalization to the Rit content for a semiquantitative measurement was used to evaluate the difference in the internalization rates of FP1, FP1-Rit, FP3 and FP3-Rit. The cells were detached from the well by incubation in a detaching solution (0.5% BSA, 10 mM EDTA, 100 mM NaCl, 20 mM HEPES, pH 7.4), centrifuged and resuspended in 0.5 mL of PBS-0.5% BSA with 5 μg mL^{-1} of Hoechst 333258. Hoechst 333258 was used to label dead cells. The samples were analyzed using FACS Verse (Becton Dickinson) and the FlowJo software. We determined the median of the fluorescence intensity of cells incubated with FP1, FP1-Rit, FP3 and FP3-Rit. As a negative control, cells that were not incubated with polymers were used.

3 Results and discussion

3.1 Design, synthesis and characterization of the polymer precursor and conjugates

The idea to use hexaleucine (Leu_6) as a hydrophobic block in the synthesis of the amphiphilic polymer carriers has arisen from our earlier unpublished results concerning the properties of a diblock copolymer consisting of poly(ethylene glycol) (M_w = 2000) and Leu_6 that formed stable micelles in a relatively broad concentration range. In this work, we designed and synthesized an A–B type diblock copolymer composed of a hydrophobic Leu_6 block (A) and a hydrophilic pHPMA-based block (B). The pseudoproline dipeptide Val-Ser($\psi^{Me,Me}$pro) was incorporated at the N-terminus of the Leu_6 sequence to improve the solubility of the product in organic solvents. To enable the growth of the hydrophilic polymer block from the Leu_6 block *via* controlled RAFT polymerization, an essential dithiobenzoate (DTB) end group was introduced at the N-terminus of the peptide to form a macrochain transfer agent specific for RAFT polymerization. In addition to the dominantly represented HPMA, the polymerization was performed in the presence of a monomer containing Boc-protected hydrazide groups (Ma-Acap-NH-NH-Boc), which enabled the attachment of Rit after the removal of the protecting Boc group. The length of the polymer hydrophilic block was controlled by modifying the molar ratio of CTA and the monomers in the reaction mixture. Thus, polymer precursors differing in the molecular weight M_w of 9000 or 25 000 g mol^{-1} were synthesized. A molecular weight below the renal threshold was selected to obtain polymers excretable from the body by glomerular filtration. The removal of the end DTB groups and the deprotection of the hydrazide groups did not change the M_w nor the dispersity ($Đ$) values. All the synthesized polymer precursors contained approximately 8.0 mol% of the hydrazide groups, which was sufficient for Rit attachment. The physicochemical characteristics of the polymer precursors and conjugates are summarized in Table 1.

The DTB-functionalized oligopeptide was prepared by solid phase peptide synthesis; therefore, the hydrophobic part of the diblock polymer was absolutely uniform in terms of molecular weight distribution. Utilizing this oligopeptide derivative as a chain transfer agent with the RAFT polymerization technique resulted in the synthesis of an amphiphilic diblock polymer with a very narrow D ($\approx$1.1).

The synthesis of the conjugates with Rit consists of the reaction of the keto group of Rit with the hydrazide groups randomly distributed in the hydrophilic part of the diblock copolymers. The reaction resulting in the hydrazone-bound Rit was not influenced by the presence of the hydrophobic peptide introduced into the polymer structure. Polymer precursors and their Rit conjugates were of similar molecular weights and dispersities, as measured by SEC in a mixture containing 20% acetate buffer and 80% methanol, which is assumed to disrupt any hydrophobic interactions. To investigate the influence of the Rit content on the self-assembly behavior of the diblock polymers, the conjugates with a lower content (approximately 3–5 wt%; P1-RitA and P2-RitA) or a higher content (approximately 10–11 wt%; P1-RitB and P2-RitB) of Rit were prepared. The hydrazone bond formed between the drug and the polymer carrier was relatively stable at pH 7.4 (approximately 5% of the released Rit within 5 h). However, it hydrolyzed rapidly at pH 5.0 and almost 90% of the Rit was released within 2 h (Fig. 1). As expected, there was no difference among the Rit release rates from the hydrophilic or amphiphilic diblock conjugates.

For the LSCM measurement, the Rit–polymer conjugates were modified with the Cyanine5.5 fluorescent dye. Because the fluorescent dye was attached to the polymer backbone through the stable diacyl diazane bond, LSCM imaging enabled the observation of the intracellular fate of the polymer carrier over time. A relatively low content of the fluorophore Cyanine5.5 (up to 1.8 wt%) was selected to maximally preserve the original physico-chemical properties and the biological behavior of the conjugates. At the same time, it was sufficient to visualize the conjugates by fluorescence confocal microscopy and by flow cytometry (FACS).

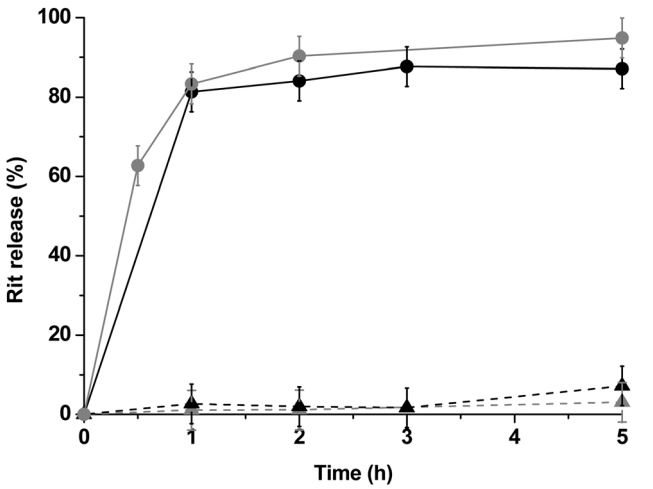

Fig. 1 The Rit release from conjugates P1-RitB (●—pH 5; ▲ - - - pH 7.4) and FP3-Rit (●—pH 5, ▲ - - - pH 7.4) in phosphate buffers of different pH values at 37 °C.

3.2 Association behavior of the copolymers in aqueous medium of various pH values

The morphology (random coil *versus* micelle) of the amphiphilic diblock copolymers in aqueous solutions can be influenced to a considerable extent by the length of the hydrophilic block, provided that the hydrophobic chain length is constant, and the amount of hydrophobic cytostatic agent (Rit) attached to it. In this work, our effort was to adjust those parameters to obtain the polymer conjugate forming micelles in an aqueous solution and disassembling into soluble unimers after the Rit release upon lowering of the pH in endosomes and lysosomes of tumor cells. Although neither of the diblock polymer precursors P1 and P2 with R_h = 2.4 nm and 4.4 nm, respectively (Table 1), formed micelles in an aqueous solution, the conjugation of 5 wt% of hydrophobic Rit to the polymer precursor P1 provided polymer conjugate P1-RitA associating into supramolecular assemblies (most probably micelles) with R_h = 11.5 nm that was almost 5 times larger than that of the polymer precursor P1. The increase in Rit content to approximately 10 wt% (P1-RitB) led to the formation of micelles with R_h = 9.6 nm. The conjugate P2-RitA, with a higher M_w of 26 200 g mol^{-1}, containing 2.5 wt% of Rit did not form micelles (R_h = 5.3 nm) because the R_h of P2-RitA did not significantly change compared to that of the corresponding precursor P2. The conjugation of 10 wt% of Rit to precursor P2 led to an increase in size to values comparable with the Rit conjugate P1-RitB, which contained the same Rit content but had a shorter hydrophilic block, suggesting the formation of micelles. However, the conjugation of 10 wt% or even 15 wt% Rit to the linear HPMA copolymer of $M_w \approx$ 25 000 g mol^{-1} without hexaleucine did not significantly change the R_h compared to the corresponding precursor (data not shown), thus leaving the conjugate water-soluble.

According to the ITC measurements, the critical micelle concentrations (CMCs) for conjugates P1-RitA and P1-RitB were 0.4 mg mL^{-1} and 0.06 mg mL^{-1}, respectively, which indicated that a higher content of hydrophobic Rit in the polymer conjugates significantly increased the stability of the micelles. Interestingly, the CMC value for P2-RitB was also 0.06 mg mL^{-1}, which suggests that the CMC values of the polymer–Rit conjugates with M_w values in the tested range mainly depended on the amount of the polymer-bound Rit. Similar results were observed previously for micelles formed by cholesterol-bearing HPMA copolymers.[26]

The stability of the micelle-forming conjugate P1-RitA and the changes in its hydrodynamic radius were evaluated during its incubation in phosphate buffers of pH 7.4 and 5.0. The conjugate incubated for 24 h in a buffer of pH 7.4 exhibited two populations of particles, a smaller one with an R_h value of approximately 14 nm and a second one with an R_h value of approximately 600 nm (Fig. 2). The smaller R_h values correspond to micelle-forming conjugates, and the larger ones to the small portion of released Rit, which is insoluble in aqueous media and forms submicron-sized aggregates. In comparison,

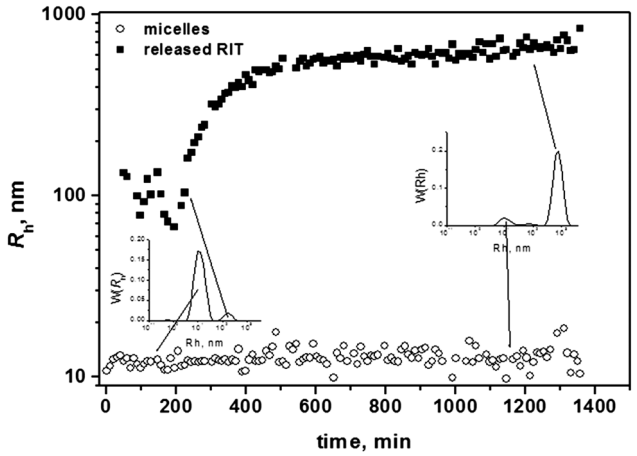

Fig. 2 The time dependence of the size of micelles and aggregates of released Rit incubated in a buffer at pH 7.4.

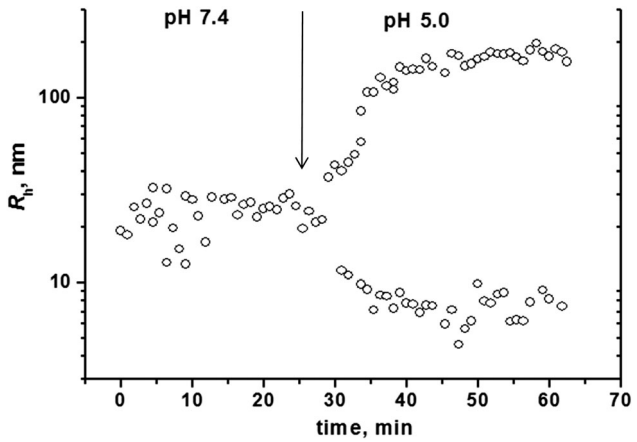

Fig. 3 Time dependence of the size of the micelles and aggregates upon the pH drop from pH 7.4 to pH 5. The arrow indicates the moment of the pH drop.

the pH decrease to 5.0 led to the rapid release of Rit, resulting in the formation of approximately 200 nm aggregates within 1 h of incubation and subsequently leading to micelle disassembly into random coil-forming polymer chains with an R_h value of approximately 5 nm, which is in accordance with the R_h values of the precursor P1 that did not form micelles (Fig. 3).

SAXS measurements confirmed the presence of micelles at pH 7.4 (Fig. 4). The $I(q)q^2$ values shown on a Kratky plot indicate a pronounced peak in a low q range. It was previously proven that the existence of such a peak is a signature of compact objects.[26] Hard spheres, micelles, and hyperbranched objects manifest as a peak on a Kratky plot (Fig. 4, inset). Less compact objects, such as a polymer coil, have a monotonous dependence as a function of q (Fig. 4, inset). The scattering data were fitted using a combined model of long cylinders and fractal aggregates implemented in the SASFit software (http://kur.web.psi.ch/sans1/SANSSoft/sasfit.html). The long cylinder model was successfully applied earlier to describe various elongated objects. Fig. 4 shows the scattering curve and the fitting

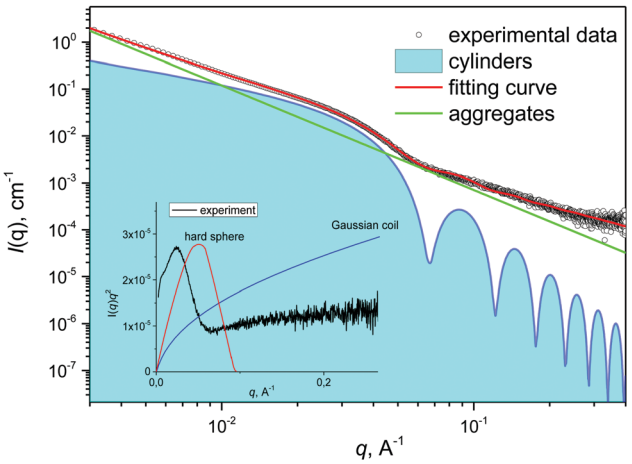

Fig. 4 Fitting of the SAXS curve for the sample P1-RitA.

function for the sample P1-RitA. The whole scattering curve from the nanoparticle can be regarded as a sum of the scattering curves of two objects, cylinders with a polydisperse length of 12 nm and a radius of 5.9 nm and aggregates with a fractal exponent value of approximately 2.2.

In addition, the micelles are formed by simply dissolving the sample in a buffer solution, which facilitates the sample preparation for further manipulation during biological testing. In contrast, the majority of polymer micelles described in the literature have a drug physically entrapped in their core. Thus, the micelle preparation is complex, and the micelles must be stored in a solution.

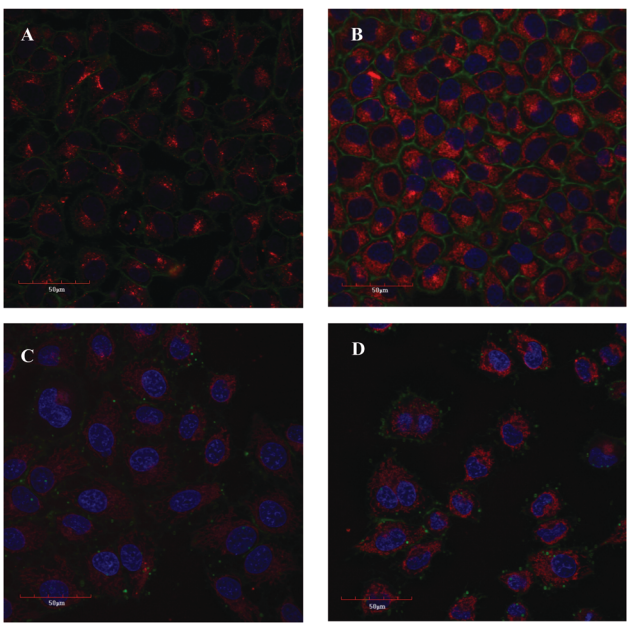

Fig. 5 Cellular uptake of polymers FP3 (A), FP3-Rit (B), FP1 (C), and FP1-Rit (D) labeled by the fluorescent dye Cyanine5.5 (colored in red). Cell membranes were stained with CellMack Green (colored green) and the nucleus was stained with Hoechst 33258 (colored blue), after incubating HeLa cells for 2 hours with fluorescently labeled polymer conjugates at 37 °C and 5% CO_2.

3.3 Cellular uptake of the polymer conjugates

To reveal the influence of both the morphology of the polymer carrier and the presence of Rit on the interaction of the polymer conjugates with living cells, we studied the cell interaction of the fluorescently labeled polymer conjugates, both with or without hexaleucine and with and without Rit, using confocal microscopy and flow cytometry.

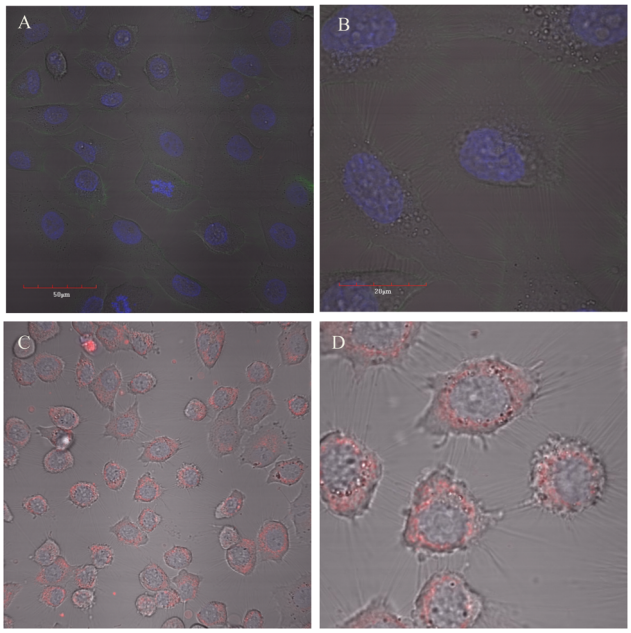

Fig. 6 Incubation of HeLa cells for 2 h with fluorescently labeled polymer conjugates at 4 °C. The uptake of the linear polymer without ritonavir, FP3 (A and B), and the linear polymer with ritonavir, FP3-Rit (C and D), labeled by the fluorescent dye Cyanine5.5 (colored in red). The nucleus was stained with Hoechst 33258 (colored blue).

3.3.1 Laser scanning confocal microscopy. Polymer conjugate internalization was evaluated after 2 h of incubation with HeLa cells. The fluorescence signal of Cyanine5.5-labeled polymers was localized in the cytoplasm of the cells. The conjugates bearing Rit, FP1-Rit and FP3-Rit, showed higher signal intensity than the conjugates without Rit, FP1 and FP3. This may correspond to more efficient and faster intracellular accumulation of the polymer conjugates with Rit (Fig. 5). We have not found any significant influence of Cyanine5.5 on the interaction or internalization of labeled polymers, FP1 and FP3, with HeLa cells. The uptake of FP1 and FP3 was such as observed previously for similar polymers labeled with other suitable dyes.

The attachment of Rit to the polymer backbone clearly enhanced the cellular uptake of the polymer conjugates. This phenomenon is more significant for the water-soluble polymer FP3-Rit without hexaleucine than for the diblock polymer FP1-Rit (Fig. 5 and 6), which could be caused by the different morphologies of the polymer conjugates and consequently, the probable steric hindrance and lower accessibility of Rit incorporated by the hydrophobic interaction in the core of micelle-forming conjugate FP1-Rit. Regarding the chemical structure, Rit may be considered a peptidomimeticum[27] that can possess similar properties to cell-penetrating peptides (CPPs).[28]

To clarify the mechanism of the enhanced cellular uptake of Rit-modified conjugates, we examined the effect of polymer bound Rit on the intracellular uptake of polymer conjugates at 4 °C, *i.e.* under the conditions excluding active transport through the cell membrane. The polymer FP3-Rit efficiently entered the cells at 4 °C. However, the internalization of FP3-Rit at 4 °C was markedly lower than the uptake at 37 °C, which may be the consequence of two possible ways of internalization, the energy-dependent and the energy-independent route. In contrast, the signals of polymers without Rit (FP3, FP1) and of the micellar conjugate FP1-Rit were not detected at 4 °C.

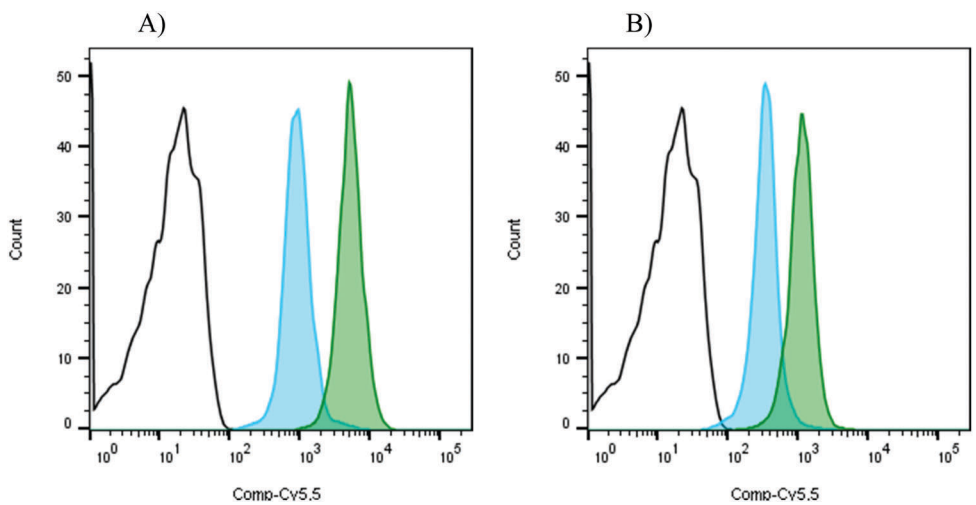

Fig. 7 Detection of the polymer conjugates labeled with Cyanine5.5 in HeLa cells by FACS. The amount of polymers was recalculated to be 12.8 μg mL^{-1} of Rit, as described in Materials and methods. (A) The fluorescence intensity histogram of non-treated HeLa cells (black histogram), cells incubated with polymer conjugates FP3 (blue histogram) and FP3-Rit (green histogram). (B) The fluorescence intensity histogram of nontreated HeLa cells (black histogram). Cells incubated with the diblock polymer conjugates FP1 (blue histogram) and FP1-Rit (green histogram).

The difference between the cellular uptake of FP3-Rit and FP1-Rit is probably influenced by the greater accessibility of Rit in the non-micellar FP3-Rit polymer conjugate to interact with the cell membrane (Fig. 5). To be precise, we have also checked the effect of free ritonavir or derivative Rit on the cellular uptake of the FP1 and FP3 polymers. We have not found any significant effect of free ritonavir or derivative Rit, when added to the cell 30 minutes before, at the same time or 30 minutes after the addition of FP3 or FP1. To sum up, there is no effect of free ritonavir or Rit on increasing uptake of the polymer conjugates.

3.3.2 Quantification of polymer conjugate uptake by flow cytometry. After 2 h of incubation with HeLa cells, the water-soluble Rit conjugate FP3-Rit without a hexaleucine block was internalized to a higher extent than the corresponding polymer without Rit (FP3), as indicated by the 5-fold higher fluorescence intensity of the conjugate FP3-Rit. Similarly, the fluorescence intensity of the internalized micelle-forming diblock Rit conjugate FP1-Rit was 2.8 times higher than that of the diblock copolymer conjugate FP1 without Rit (Fig. 7). The data agree well with the results from the LSCM analysis, where the strongest intracellular signal was observed in the cells incubated with the non-micellar polymer Rit conjugate FP3-Rit. The difference in the cellular uptake of the linear and micellar polymer Rit conjugates could be caused by the different architectures of the conjugates and the "stealthing" Rit in the micelle core, which may affect its accessibility to interact with the cell membrane.

4 Conclusions

We successfully designed and synthesized amphiphilic diblock polymer conjugates of the cytostatic agent Rit covalently linked to the polymer carrier *via* an acid labile hydrazone bond. The diblock polymer consisted of a short hydrophobic oligopeptide based on hexaleucine and a hydrophilic block composed of HPMA-based copolymer enabling the attachment of hydrophobic Rit. The combination of solid phase peptide synthesis with the RAFT polymerization technique resulted in the preparation of an amphiphilic diblock polymer with a well-defined molecular weight and a molecular weight distribution close to 1. Although the diblock polymer precursors did not self-assemble and remained water-soluble, the amphiphilic diblock polymer Rit conjugate with M_w = 12 800 g mol^{-1} did form micelles with a R_h value of approximately 10 nm and a CMC value of 0.06 mg mL^{-1}. The Rit conjugates with a longer hydrophilic polymer chain (M_w = 27 400 g mol^{-1}) formed micelles in aqueous solution only when the content of Rit was higher than 10 wt%. These micelles were relatively stable at pH 7.4 (20% of Rit within was released within 24 h at 37 °C), corresponding to conditions during transport in blood, but they dissociated rapidly at a mildly acidic pH because of the very fast release of Rit from the polymer carrier (almost 90% of Rit was released within 1 h at pH 5.0 at 37 °C, modeling conditions in the endosomes of tumor cells). Therefore, it can be expected that the micelle-forming diblock conjugates with Rit can accumulate to a higher extent in tumor tissue than the smaller Rit conjugate without hexaleucine because of the EPR effect. Moreover, after the release of Rit in tumor tissue/cells, and subsequently after its disassembly into unimers, the polymer carrier can be excreted easily from the organism by glomerular filtration.

Interestingly, the study concerning the interaction of the polymer conjugates with HeLa cells revealed the ability of polymer-bound Rit to enhance the cellular uptake of the conjugates compared to the corresponding polymers without Rit. Enhanced uptake was observed using both Rit conjugates; however, the effect was less pronounced for the micellar diblock conjugate in which the Rit molecules may be less accessible for interaction with the cellular membrane. Surprisingly, the cell internalization was active even at 4 °C, *i.e.* under conditions excluding the endocytosis of the polymer conjugate, thus proving that it requires the rather active mechanism of transport through the membrane. A detailed study concerning the influence of the polymer-bound Rit on the expression of genes involved in endocytosis at both the genomic and proteomic levels is in progress.

We believe that the pH-sensitive micelle-forming diblock polymer conjugates with Rit may be used for the problematic administration of ritonavir as a potential anticancer agent. These micelle-forming Rit conjugates might significantly improve the complicated treatment of malignancies including the highly resistant types. Further *in vitro* and *in vivo* experiments are under way.

Acknowledgements

This work was supported by the Ministry of Education, Youth and Sports of the Czech Republic within the National Sustainability Program I (Project POLYMAT LO1507) and by the Czech Science Foundation (project No. P301/12/1254, 15-02986S and 16-17207S).

References

1 J. Yang and J. Kopecek, Macromolecular therapeutics, *J. Controlled Release*, 2014, **190**, 288–303.
2 H. Maeda, H. Nakamura and J. Fang, The EPR effect for macromolecular drug delivery to solid tumors: Improvement of tumor uptake, lowering of systemic toxicity, and distinct tumor imaging *in vivo*, *Adv. Drug Delivery Rev.*, 2013, **65**, 71–79.
3 V. Torchilin, Tumor delivery of macromolecular drugs based on the EPR effect, *Adv. Drug Delivery Rev.*, 2011, **63**, 131–135.
4 H. Maeda, Macromolecular therapeutics in cancer treatment: the EPR effect and beyond, *J. Controlled Release*, 2012, **164**, 138–144.
5 J. Kopeček and P. Kopečková, HPMA copolymers: origins, early developments, present, and future, *Adv. Drug Delivery Rev.*, 2010, **62**, 122–149.
6 H. S. Yoo and T. G. Park, Folate receptor targeted biodegradable polymeric doxorubicin micelles, *J. Controlled Release*, 2004, **96**, 273–283.

7 T. Etrych, M. Šírová, L. Starovoytova, B. Říhová and K. Ulbrich, HPMA copolymer conjugates of paclitaxel and docetaxel with pH-controlled drug release, *Mol. Pharmaceutics*, 2010, **7**, 1015–1026.
8 H. Nakamura, T. Etrych, P. Chytil, M. Ohkubo, J. Fang, K. Ulbrich and H. Maeda, Two step mechanisms of tumor selective delivery of *N*-(2-hydroxypropyl)methacrylamide copolymer conjugated with pirarubicin *via* an acid-cleavable linkage, *J. Controlled Release*, 2014, **174**, 81–87.
9 E. Y. Moawad, Identifying the optimal dose of ritonavir in the treatment of malignancies, *Metab. Brain Dis.*, 2014, **29**, 533–540.
10 A. Srirangam, M. Milani, R. Mitra, Z. Guo, M. Rodriguez, H. Kathuria, S. Fukuda, A. Rizzardi, S. Schmechel, D. G. Skalnik, L. M. Pelus and D. A. Potter, The HIV Protease Inhibitor Ritonavir Inhibits Lung Cancer Cells, in part, by Inhibition of Survivin, *J. Thorac. Oncol.*, 2011, **6**, 661–670.
11 S. Kumar, C. S. Bryant, S. Chamala, A. Qazi, S. Seward, J. Pal, C. P. Steffes, D. W. Weaver, R. Morris, J. M. Malone, M. A. Shammas, M. Prasad and R. B. Batchu, Ritonavir blocks AKT signaling, activates apoptosis and inhibits migration and invasion in ovarian cancer cells, *Mol. Cancer*, 2009, **8**, 26.
12 V. Šubr, L. Sivák, E. Koziolová, A. Braunová, M. Pechar, J. Strohalm, M. Kabešová, B. Říhová, K. Ulbrich and M. Kovář, Synthesis of Poly[*N*-(2-hydroxypropyl)methacrylamide] Conjugates of Inhibitors of the ABC Transporter That Overcome Multidrug Resistance in Doxorubicin-Resistant P388 Cells in Vitro, *Biomacromolecules*, 2014, **15**, 3030–3043.
13 T. Etrych, L. Kovář, J. Strohalm, P. Chytil, B. Říhová and K. Ulbrich, Biodegradable star HPMA polymer–drug conjugates: Biodegradability, distribution and anti-tumor efficacy, *J. Controlled Release*, 2011, **154**, 241–248.
14 K. Miyata, R. J. Christie and K. Kataoka, Polymeric micelles for nano-scale drug delivery, *React. Funct. Polym.*, 2011, **71**, 227–234.
15 M. Talelli, C. J. Rijcken, C. F. van Nostrum, G. Storm and W. E. Hennink, Micelles based on HPMA copolymers, *Adv. Drug Delivery Rev.*, 2010, **62**, 231–239.
16 Q. Zhang, N. Re Ko and J. Kwon Oh, Recent advances in stimuli-responsive degradable block copolymer micelles: synthesis and controlled drug delivery applications, *Chem. Commun.*, 2012, **48**, 7542–7552.
17 Č. Koňák, D. Oupický, V. Chytrý, K. Ulbrich and M. Helmstedt, Thermally Controlled Association in Aqueous Solutions of Diblock Copolymers of Poly[*N*-(2-hydroxypropyl)-methacrylamide] and Poly(*N*-isopropylacrylamide), *Macromolecules*, 2000, **33**, 5318–5320.
18 C.-Y. Hong and C.-Y. Pan, Direct Synthesis of Biotinylated Stimuli-Responsive Polymer and Diblock Copolymer by RAFT Polymerization Using Biotinylated Trithiocarbonate as RAFT Agent, *Macromolecules*, 2006, **39**, 3517–3524.
19 A. P. Griset, J. Walpole, R. Liu, A. Gaffey, Y. L. Colson and M. W. Grinstaff, Expansile nanoparticles: synthesis, characterization, and *in vivo* efficacy of an acid-responsive polymeric drug delivery system, *J. Am. Chem. Soc.*, 2009, **131**, 2469–2471.
20 Y. Zhao, Light-Responsive Block Copolymer Micelles, *Macromolecules*, 2012, **45**, 3647–3657.
21 N. V. Tsarevsky and K. Matyjaszewski, Reversible redox cleavage/coupling of polystyrene with disulfide or thiol groups prepared by atom transfer radical polymerization, *Macromolecules*, 2002, **35**, 9009–9014.
22 P. Chytil, T. Etrych, J. Kříž, V. Šubr and K. Ulbrich, *N*-(2-Hydroxypropyl)methacrylamide-based polymer conjugates with pH-controlled activation of doxorubicin for cell-specific or passive tumour targeting. Synthesis by RAFT polymerisation and physicochemical characterisation, *Eur. J. Pharm. Sci.*, 2010, **41**, 473–482.
23 K. Ulbrich, T. Etrych, P. Chytil, M. Jelínková and B. Říhová, Antibody-targeted polymer-doxorubicin conjugates with pH-controlled activation, *J. Drug Targeting*, 2004, **12**, 477–489.
24 S. Perrier, P. Takolpuckdee and C. A. Mars, Reversible addition-fragmentation chain transfer polymerization: End group modification for functionalized polymers and chain transfer agent recovery, *Macromolecules*, 2005, **38**, 2033–2036.
25 T. Etrych, T. Mrkvan, P. Chytil, Č. Koňák, B. Říhová and K. Ulbrich, *N*-(2-hydroxypropyl)methacrylamide-based polymer conjugates with pH-controlled activation of doxorubicin. I. New synthesis, physicochemical characterization and preliminary biological evaluation, *J. Appl. Polym. Sci.*, 2008, **109**, 3050–3061.
26 S. K. Filippov, P. Chytil, P. V. Konarev, M. Dyakonova, C. Papadakis, A. Zhigunov, J. Pleštil, P. Štěpánek, T. Etrych, K. Ulbrich and D. I. Svergun, Macromolecular HPMA-Based Nanoparticles with Cholesterol for Solid-Tumor Targeting: Detailed Study of the Inner Structure of a Highly Efficient Drug Delivery System, *Biomacromolecules*, 2012, **13**, 2594–2604.
27 J. T. Randolph and D. A. DeGoey, Peptidomimetic inhibitors of HIV protease, *Curr. Top. Med. Chem.*, 2004, **4**, 1079–1095.
28 D. M. Copolovici, K. Langel, E. Eriste and U. Langel, Cell-penetrating peptides: design, synthesis, and applications, *ACS Nano*, 2014, **8**, 1972–1994.